frontiers | Frontiers in Mechanical Engineering

TYPE Original Research
PUBLISHED 27 November 2024
DOI 10.3389/fmech.2024.1504347

OPEN ACCESS

EDITED BY
Andras Vernes,
Vienna University of Technology, Austria

REVIEWED BY
Michał Stosiak,
Wroclaw University of Science and Technology, Poland
Milan Bukvic,
University of Kragujevac, Serbia

*CORRESPONDENCE
Shunsuke Iwase,
iwase-sh@nsk.com

RECEIVED 30 September 2024
ACCEPTED 07 November 2024
PUBLISHED 27 November 2024

CITATION
Iwase S, Maruyama T, Momozono S, Maegawa S and Itoigawa F (2024) Studies on dielectric spectroscopy of oxidatively degraded Poly(α-olefin).
Front. Mech. Eng. 10:1504347.
doi: 10.3389/fmech.2024.1504347

Studies on dielectric spectroscopy of oxidatively degraded Poly(α-olefin)

Shunsuke Iwase[1,2,3]*, Taisuke Maruyama[1,2], Satoshi Momozono[1,2], Satoru Maegawa[3] and Fumihiro Itoigawa[3]

[1]Core Technology R&D Center, NSK Ltd., Fujisawa, Japan, [2]NSK Tribology Collaborative Research Cluster, Tokyo Institute of Technology, Yokohama, Japan, [3]Nagoya Institute of Technology, Nagoya, Japan

Failures in tribological components such as bearings can significantly affect the performance and lifespan of machinery, necessitating the implementation of effective condition monitoring technologies. This study verified the feasibility of dielectric spectroscopy (DES) as a method for detecting abnormalities before damage occurs. A comparative evaluation was conducted between dielectric relaxation parameters and measurements from size exclusion chromatography, total acid number, and viscosity for oxidatively degraded poly (α-olefin) oils. The results confirmed that DES is an effective method for assessing the oxidative degradation state of lubricants. These findings suggest that DES could be applied to oil film condition monitoring and predictive maintenance.

KEYWORDS

dielectric spectroscopy, lubricants, oil, degradation, electrical impedance method, condition monitoring, oil diagnosis

1 Introduction

Failures in tribological components such as bearings have a significant impact on the overall performance and lifespan of machinery, necessitating the implementation of appropriate condition monitoring technologies. Traditionally, abnormal vibration sensing has been widely employed to monitor the condition of bearings (Kiral and Karagülle, 2003; Al-Badour et al., 2011; Zarei et al., 2014; Cambow et al., 2018). However, abnormal vibrations typically manifest as a result of damage caused by lubrication failure at the sliding surfaces, and by the time such vibrations are detected, component replacement is often required. In contrast, monitoring the condition of the lubricating oil film offers the potential to detect abnormalities before surface damage occurs. If this method is established, it could allow for methods other than part replacement, such as lubricant replacement, leading to significant reductions in maintenance costs. Additionally, it could serve as a means to identify the specific causes of failure within components, such as incorrect lubricant selection or improper design and installation methods. While optical techniques, such as optical interferometry (Johnston et al., 1991; Kaneta et al., 1993; Sugimura et al., 1998; Maruyama and Saitoh, 2010), are commonly used for monitoring oil films, they cannot be applied to metal components. Therefore, electrical methods have gained attention as potential oil film monitoring techniques for metal-to-metal sliding surfaces.

The capacitance method calculates oil film thickness from the film capacitance and can be applied to thin oil films, ranging from tens to hundreds of nanometers, formed under EHL (elastohydrodynamic lubrication) conditions (Crook, 1961; Prashad, 1988; Jablonka

et al., 2012). Moreover, the impedance method, which builds upon the capacitance technique, allows for high-precision oil film thickness measurement and simultaneously provides information on metal contact (Nakano and Akiyama, 2006; Manabe and Nakano, 2008; Nihira et al., 2015; Schnabel et al., 2016; Maruyama and Nakano, 2018). Consequently, this method has been actively studied in recent years as a predictive maintenance (PdM) technique for rolling bearings (Becker-Dombrowsky and Kirchner, 2024; Maruyama and Nakano, 2018; Maruyama et al., 2024).

Thus, monitoring oil film thickness using electrical methods is considered a promising advanced condition monitoring technology for bearings, but it does not predict lubrication failure leading to metal contact. Generally, lubrication failure is caused by factors such as a decrease in lubricant quantity due to leakage or evaporation, as well as changes in lubricant properties caused by oxidation degradation or contamination. In particular, when lubricant oxidation progresses, it is expected that while the oil film may temporarily thicken due to the increased viscosity of the lubricant based on the Hamrock and Dowson theory (Hamrock and Dowson, 1977), it may simultaneously undergo viscosity reduction due to a rise in temperature caused by increased shear resistance. In other words, monitoring only oil film thickness may not allow for the prediction of damage due to lubrication failure until just before it occurs. If changes in the chemical properties of the lubricant, such as viscosity or acid number, can be monitored, it may become possible to predict the time remaining until lubrication failure during the steady state, when changes in oil film thickness are minimal, thus enabling the realization of PdM for bearings. This means that condition-based maintenance can be implemented, rather than the conventional time-based maintenance. For bearings equipped with oil circulation systems, sensors capable of monitoring lubricant degradation can be installed within the circulation mechanism, making it possible to apply previously reported diagnostic techniques (Patocka et al., 2020). However, particularly in the case of rolling bearings, the lubricant is often sealed, leaving no space to insert a sensor. Therefore, direct sensing in the oil film area is more desirable.

Although there are currently no reported methods for monitoring the chemical property changes of lubricants in oil films formed between metal sliding surfaces, it is possible that existing electrical measurement techniques for bulk lubricants between parallel electrodes could be adapted. Dielectric spectroscopy (DES), which observes the AC frequency response of the complex permittivity, provides direct information on molecular dynamics, making it a promising measurement technique for monitoring chemical property changes, such as lubricant degradation. Guan et al. reported that the total acid number (TAN) and sludge content could be predicted by analyzing DES measurement data (Guan et al., 2011). Additionally, Gong et al. stated that the quantification of nitrogen compounds and sulfur oxides generated in the oil could be achieved by analyzing the temperature dependence of the complex permittivity obtained from two-dimensional DES measurements (Gong et al., 2016; Gong et al., 2017).

However, DES measurements of lubricants reported so far have mainly focused on degradation state prediction based on statistical analysis, and a systematic theoretical framework regarding the underlying physical mechanisms has not yet been sufficiently established. Thus, the challenges associated with applying DES to oil film monitoring remain unclear.

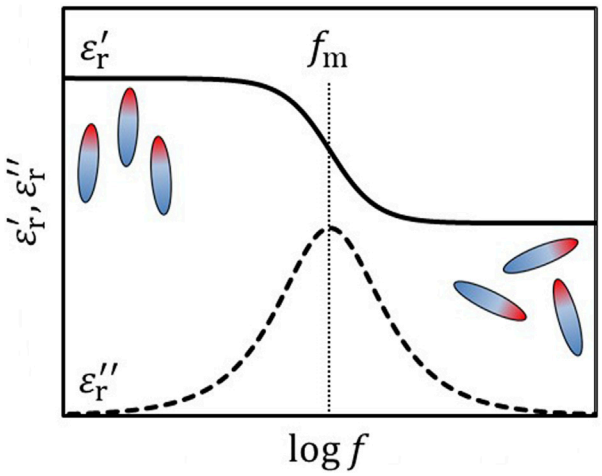

FIGURE 1
Conceptual diagram of DES measurement.

Therefore, in this study, we aim to utilize DES measurements of oil films for the PdM of bearings and consider the information obtained from DES measurements of lubricants under static conditions from the perspective of dielectric relaxation theory. Specifically, we conduct DES measurements of degraded oils using parallel plate capacitors and discuss the relationships between the dielectric properties obtained and the concentration of degradation products, molecular weight, kinematic viscosity, and TAN obtained from various chemical analyses. Additionally, we will discuss the potential for applying oil film DES measurements to PdM and the challenges involved. The insights gained from this report on the dielectric relaxation properties of oils associated with lubricant degradation will contribute to advancements in lubricant degradation monitoring technology for tribological components, further supporting the realization of PdM.

2 Experimental details

In this section, we explain the principles and techniques of dielectric spectroscopy. We also explore various models used to describe the relaxation phenomena observed in the frequency characteristics of complex permittivity obtained through measurement, and provide a detailed explanation of the fitting methods applied to these models.

2.1 DES and dielectric relaxation

Except for purely non-polar oils, most lubricants contain polar molecules within their components. Examples of such components include ester-based oils, grease thickeners, certain additives, and oxidative degradation products of lubricants. The complex permittivity ε^* [F/m] of materials that contain internal polar

10.3389/fmech.2024.1504347

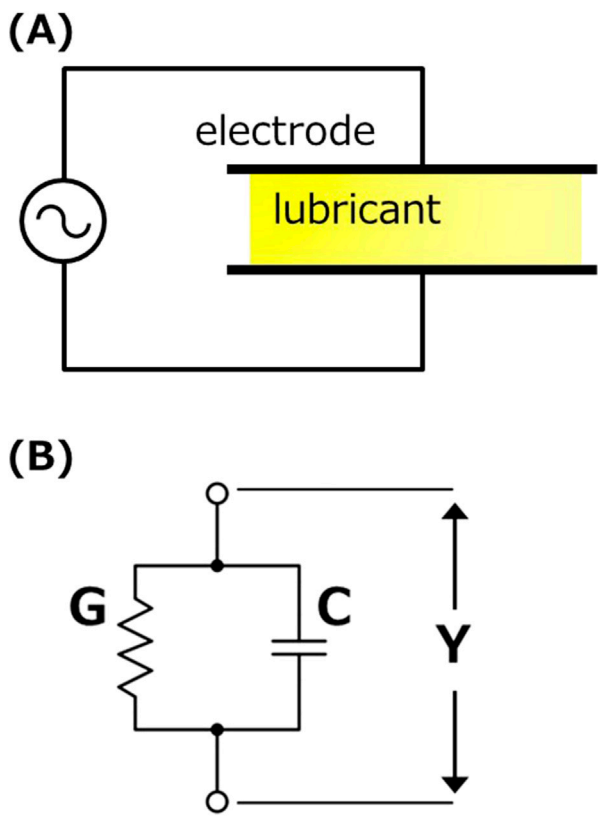

FIGURE 2
DES measurement method for lubricants, **(A)** Schematic diagram, **(B)** Equivalent circuit.

molecules, i.e., permanent dipoles, is expressed by the following equation. For the derivation of this equation, please refer to the relevant literature (Böttcher and Bordewijk, 1980).

$$\frac{\varepsilon^*}{\varepsilon_0} = \varepsilon_r^* = \varepsilon_r' - j\varepsilon_r'' \tag{1}$$

Here, ε_r^* [-] represents the complex relative permittivity. The real part, ε_r' [-], is referred to as the storage permittivity, or simply the relative permittivity. The imaginary part, ε_r'' [-], is commonly known as the dielectric loss factor.

Dielectric relaxation refers to the phenomenon where polarization of a dielectric material lags behind the applied alternating electric field. Dielectric relaxation appears as the frequency characteristics of complex permittivity in DES measurements. An example of DES measurements is shown in Figure 1.

In the low-frequency region, the permanent dipoles align with the external electric field, resulting in a high ε_r' value. As the frequency increases, the permanent dipoles gradually fail to follow the polarity reversals of the external electric field, and at sufficiently high frequencies, ε_r' asymptotically approaches a low value. ε_r'' reaches its maximum value at the relaxation frequency f_m, which corresponds to the inflection point of ε_r'. The relaxation time τ is expressed as $\tau = 1/2\pi f_m$ and represents the time required for the dipoles to reorient.

The equivalent circuit for dielectric spectroscopy measurements of lubricants using parallel plate electrodes is shown in Figure 2.

Since lubricants may exhibit conductivity due to additives or oxidation degradation products, they should be considered as a parallel circuit of a capacitor and a resistor. The complex admittance Y [S] of the dielectric material inserted between the electrodes is generally expressed using conductance G [S] and capacitance C [F] by the following equation.

$$Y = G + j\omega C \tag{2}$$

Here, ω [rad/s] represents the angular frequency, and using the alternating current frequency f [Hz], ω is expressed as $\omega = 2\pi f$. Furthermore, Equation 2 can be expressed in terms of the electrode area S [m^2] and the distance between the electrodes d [m] as follows.

$$Y = \left(\sigma_0 + \omega\left(\varepsilon_a'' + j\varepsilon'\right)\right)\frac{S}{d} \tag{3}$$

Here, σ_0 [S/m] represents the DC conductivity, and ε_a'' [F/m] denotes the absorptive dielectric loss caused by relaxation. Additionally, the complex admittance Y can also be expressed using the complex impedance Z [Ω], which is obtained through measurements, as follows.

$$Y = \frac{1}{Z} = \frac{\cos\theta}{|Z|} - j\frac{\sin\theta}{|Z|} \tag{4}$$

Here, $|Z|$ [Ω] represents the magnitude of the impedance of the measured object, and θ [deg] denotes the phase difference between the applied voltage and the response current. By comparing the real and imaginary parts of Equations 3, 4, Equations 5, 6 can be derived.

$$\varepsilon_r' = -\frac{d\sin\theta}{S\omega|Z|\varepsilon_0} \tag{5}$$

$$\frac{\sigma_0}{\omega\varepsilon_0} + \frac{\varepsilon_a''}{\varepsilon_0} = \varepsilon_r'' = \frac{d\cos\theta}{S\omega|Z|\varepsilon_0} \tag{6}$$

The first term on the left-hand side of Equation 6 represents the conductive dielectric loss due to the conductive component. The equation including the conductive dielectric loss term is also described in the review by Woodward et al.; for further details, please refer to that source (Woodward, 2021).

2.2 Curve fitting

In this report, the Cole-Cole relaxation model was adopted to describe the relaxation phenomena. The Cole-Cole relaxation equation is a semi-empirical extension of the theoretical Debye relaxation equation and is commonly used in the analysis of dielectric relaxation (Kremer and Schönhals, 2003). However, the Cole-Cole model addresses only absorptive losses and does not take conductive losses into account. Specifically, it does not include the contribution of the first term on the left-hand side of Equation 6. As mentioned earlier, the conductivity of lubricants, which emerges due to oxidative degradation, can serve as an important indicator for estimating lubricant degradation. Therefore, in this study, the Cole-Cole relaxation

TABLE 1 Test oil properties.

Oil	Sample ID	Heating time [hour]	TAN [KOH mg/g]	Kinematic viscosity [mm²/s]		
				At 40°C	At 70°C	At 100°C
Low viscosity PAO	L0	0[a]	–[b]	30	11	6
	L1	139	4.0	51	17	8
	L2	333	6.9	98	28	12
	L3	446[c]	12.1	–[b]	106	35
High viscosity PAO	H0	0[a]	–[b]	124	43	20
	H1	139	3.1	180	57	24
	H2	333	4.6	352	90	35
	H3	446[c]	8.8	–[b]	375	117

[a]New oil was used.
[b]No data available as the value fell below the measurement limit.
[c]To accelerate degradation, the sample amount in the beaker was reduced by half before heating.

model was directly applied to fit ε_r' (Equation 7), while for fitting ε_r'', a modified version of the Cole-Cole equation with an added term for conductive losses was used (Equation 8).

$$\varepsilon_r{}' = \varepsilon_{r\infty} + \frac{\Delta\varepsilon}{2}\left(1 - \frac{\sinh\beta x}{\cosh\beta x + \cos(\beta\pi/2)}\right) \tag{7}$$

$$\varepsilon_r{}'' = \frac{\sigma_0}{\omega\varepsilon_0} + \frac{\Delta\varepsilon}{2}\frac{\sin(\beta\pi/2)}{\cosh\beta x + \cos(\beta\pi/2)} \tag{8}$$

where $x = \ln 2\pi f\tau$. Here, $\varepsilon_{r\infty}$, $\Delta\varepsilon$, τ, β and σ_0 are fitting parameters, which are explained in detail in Section 4.1. By using these equations, the behavior of dielectric relaxation and the changes in conductivity can be simultaneously evaluated.

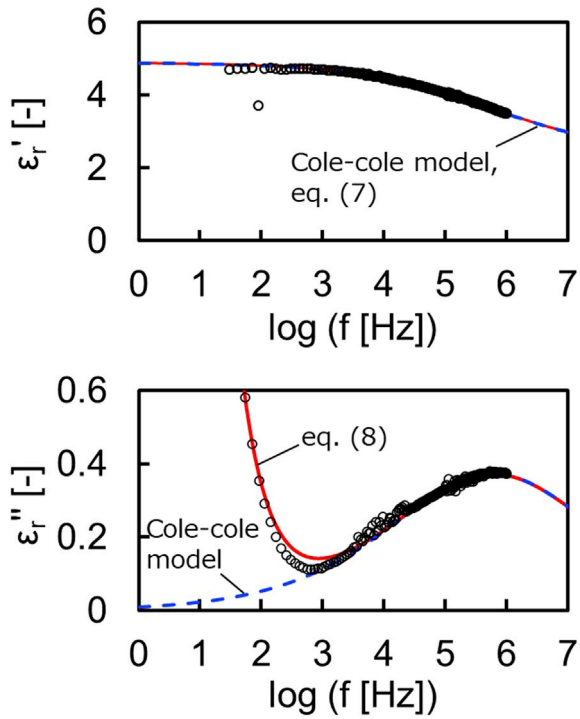

FIGURE 3
Curve fitting results of ε_r' and ε_r''; The black circle plot shows the dielectric spectroscopy measurements of L3. The red solid line represents the fitting results using Equations 6, 7. The blue dashed line represents the fitting results using the Cole-Cole relaxation model.

3 Experimental method

3.1 Materials

In this experiment, two types of PAO (Poly (α-olefin)) with different viscosities were used. Each sample was placed in a glass beaker and subjected to thermal degradation by heating in an oven at 160°C. The heating duration and kinematic viscosity of each sample are presented in Table 1. Additionally, the values of TAN, which is commonly used as an indicator of oxidative degradation, are also provided.

3.2 Apparatus

The electrodes used in this study were Keysight 16452A. The electrode material was nickel-plated kovar (Fe: 54%, Co.: 17%, Ni: 29%), with an electrode gap of 0.3 mm and an electrode diameter of 38 mm. Complex impedance was measured using the HIOKI IM3536 impedance analyzer. For kinematic viscosity measurements, the Omnitek S-flow 1,200 capillary viscometer was used, following ASTM D445. The total acid number (TAN) was measured according to ASTM D 664, with automatic titration performed using the HIRANUMA COMTITE-550. SEC (size exclusion chromatography) measurements were carried out using the Nexera™ GPC System by Shimadzu, with a Shodex 803L column. Tetrahydrofuran was used as the measurement solvent. A refractive index detector was employed, and the molecular weights were calculated using polyethylene standards for calibration.

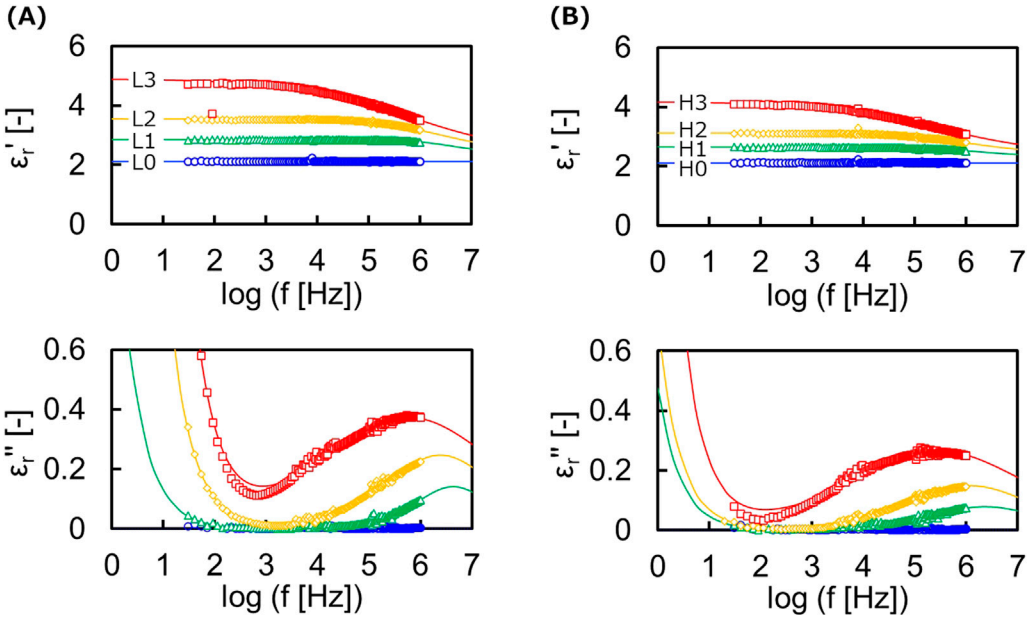

FIGURE 4
The ε_r' and ε_r'' obtaind from DES measurement; **(A)** Low viscosity PAO: blue circle plot, green triangle plot, yellow diamond plot, and red square plot represent the measurements of L0, L1, L2, and L3, respectively. **(B)** High viscosity PAO: blue circle plot, green triangle plot, yellow diamond plot, and red square plot represent the measurements of H0, H1, H2, and H3, respectively. The solid lines in the figures represent curve fittings based on Equations 7, 8.

3.3 Measurement procedure for DES

The complex impedance was obtained using the apparatus described in Section 3.2 and measured by the four-terminal pair method. The applied voltage was set to 1 V, and the AC frequency was swept from 30 Hz to 1 MHz. The cell temperature during measurement was monitored with a thermocouple and maintained at 20°C for all experiments. Moreover, preliminary evaluations confirmed that the variation in complex impedance measurements is negligibly small, with minimal impact on the results. Consequently, all data presented in this paper were derived from a single measurement.

4 Results

4.1 DES measurements

From the values of TAN and kinematic viscosity shown in Table 1, it can be seen that the degree of oxidative degradation of the prepared samples increased in the order of L0 < L1 < L2 < L3 for the low viscosity oil, and H0 < H1 < H2 < H3 for the high viscosity oil.

Figure 3 shows an example of DES measurements (sample L3) and the results of curve fitting.

When using the Cole-Cole relaxation model, a significant deviation in ε_r'' was observed in the low-frequency region. However, by using Equation 8, a good fit was obtained for ε_r'' across the entire frequency range. This allowed for the quantification of the relaxation parameters $\varepsilon_{r\infty}$ [-], $\Delta\varepsilon$ [-], τ [s], β [-], and σ_0 [S/m]. Here, $\varepsilon_{r\infty}$ represents the permittivity at the high-frequency limit, and $\Delta\varepsilon$ corresponds to the relaxation strength (the difference between the static permittivity and $\varepsilon_{r\infty}$, i.e., the peak height). τ is the relaxation time, which, as mentioned earlier, depends on the frequency at the peak of ε_r''. β represents the distribution of relaxation times and takes a value between 0 and 1; the closer β is to 0, the broader the relaxation peak. σ_0 is the DC conductivity, and the larger the value, the greater the increase in ε_r'' in the low-frequency region.

TABLE 2 Relaxation parameters of degraded PAO obtained from curve fitting.

	L1	L2	L3	H1	H2	H3
$\varepsilon_{r\infty}$ [−]	2.40	2.48	2.36	2.30	2.40	2.36
$\Delta\varepsilon$ [−]	0.44	1.08	2.54	0.35	0.72	1.82
τ [μs]	0.037	0.066	0.27	0.069	0.13	0.52
β [−]	0.73	0.55	0.36	0.55	0.50	0.36
σ_0 [nS/m]	0.07	0.52	1.3	0.02	0.04	0.11

Figure 4A shows the DES measurement results for low viscosity PAO, and Figure 4B shows those for high viscosity PAO. In the undegraded state (L0, H0), ε_r' remained constant across all frequencies, and ε_r'' was 0 across the entire frequency range. In the oxidatively degraded samples (L1, L2, L3, H1, H2, H3), dielectric relaxation was observed. In addition, high-precision curve fitting was applied to all samples. The relaxation parameters obtained from the fitting are shown in Table 2. As degradation progressed, $\Delta\varepsilon$, τ, and σ_0 increased, while β decreased.

4.2 SEC analysis

SEC measurements were conducted to obtain information on the molecular weight and concentration of components generated

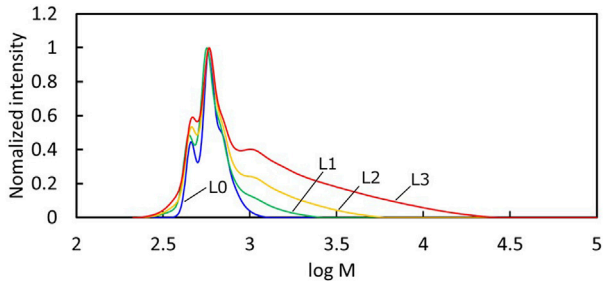

FIGURE 5
SEC results of low viscosity PAO; blue, green, yellow, and red line represent the measurements of L0, L1, L2, and L3, respectively.

TABLE 3 Parameters of degraded components obtained from SEC.

	L1	L2	L3	H1	H2	H3
C_d [g/mL]	0.27	0.42	0.64	0.19	0.35	0.55
M_w [–]	810	1,300	2,600	2,210	4,710	11,210
PDI [–]	1.3	1.5	2.2	2.3	3.4	6.2

by degradation. The results of the SEC measurements for low viscosity PAO are shown in Figure 5. The intensity shown on the vertical axis in Figure 5 was normalized using the peak derived from the fresh component detected around log M = 2.8. Compared to the undegraded sample (L0), an increase in high molecular weight components was observed as degradation progressed. The calculated values of the mass concentration of degraded components, C_d [g/mL], weight-average molecular weight, M_w [-], and polydispersity index, PDI [-], are presented in Table 3. The methods used for C_d, M_w, and PDI are described in the Supplementary Information.

5 Discussion

DES measurements were conducted on oxidatively degraded PAO. As the oxidative degradation progressed, changes were observed in the relaxation strength, $\Delta\varepsilon$, relaxation time, τ, relaxation time distribution parameter, β, and DC conductivity, σ_0. In the following sections, the changes in each of these relaxation parameters are discussed using the results from SEC, TAN, and viscosity measurements.

5.1 Relationship between $\Delta\varepsilon$ and C_d

$\Delta\varepsilon$ is generally known to be proportional to the number of dipoles per unit volume (Kremer and Schönhals, 2003), as shown in Equation 9.

$$\Delta\varepsilon = \frac{1}{3\varepsilon_0}\frac{\mu^2}{k_B T}\frac{N}{V} \tag{9}$$

Here, k_B, T, μ, N and V represent the Boltzmann constant, absolute temperature, magnitude of dipole moment, number of dipoles, and volume, respectively. Figure 6 illustrates the relationship between $\Delta\varepsilon$ and the mass concentration of degradation products, C_d.

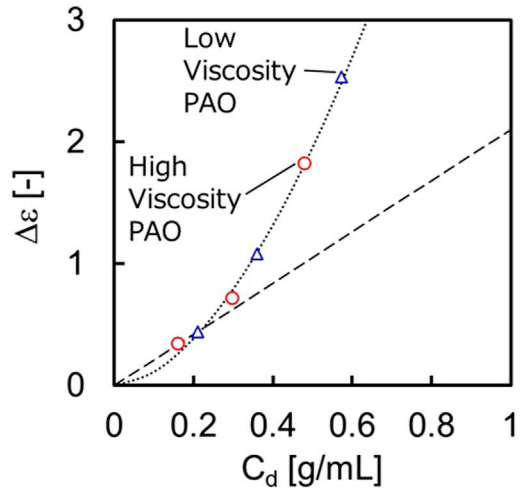

FIGURE 6
Relationship between $\Delta\varepsilon$ and C_d; Red circles represent samples H1, H2, and H3, while blue triangles represent samples L1, L2, and L3.

For the two points in the region where C_d is small (H1, L1), a proportional relationship between $\Delta\varepsilon$ and C_d was observed. However, in the region where C_d is large, $\Delta\varepsilon$ exhibited a regular change, approximately following the square of C_d. According to studies by Onsager and Kirkwood, it has been reported that when the dipole concentration in a system is high, interactions between the relaxation species become prominent, leading to an increase in $\Delta\varepsilon$ (Böttcher and Bordewijk, 1973). Although the detailed mechanism remains open to further discussion, it has been demonstrated that, at least for PAO-based oils, the concentration of degradation products can be calculated as a simple power function using $\Delta\varepsilon$ obtained from DES measurements, regardless of the initial oil viscosity.

5.2 Relationship between τ and η

According to Debye's theory (Debye, 1929), τ is expressed by the following equation.

$$\tau = \frac{4\pi R^3}{k_B T}\eta \tag{10}$$

Here, R represents the effective radius of the dipole. While η generally refers to the solvent viscosity, Iwamoto et al. reported that when the solute concentration is high, the interactions between solute molecules become stronger, and it is preferable to use the solution viscosity (Iwamoto and Kumagai, 1998). Therefore, the relationship between the relaxation time τ obtained from DES and the solution viscosity η of each sample was evaluated. η was calculated by converting the kinematic viscosity at each temperature (Table 1) to the viscosity at 20°C using Walther's equation, and then multiplying by the measured density (see

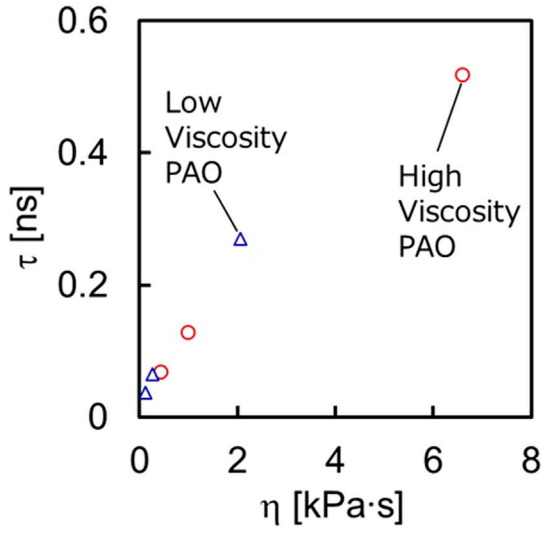

FIGURE 7
Relationship between τ and η; Red circles represent samples H1, H2, and H3, while blue triangles represent samples L1, L2, and L3.

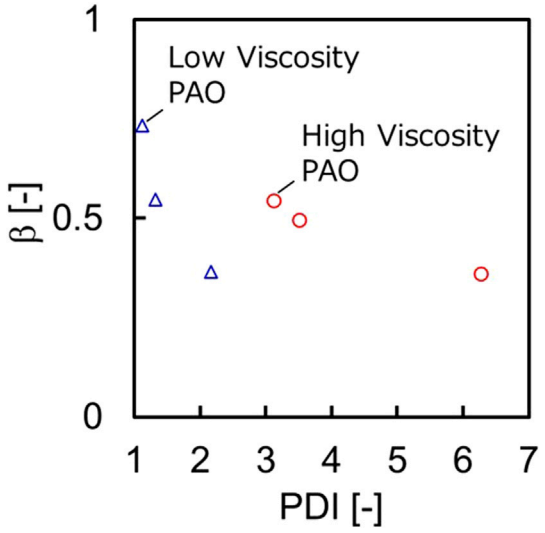

FIGURE 9
Relationship between β and PDI; Red circles represent samples H1, H2, and H3, while blue triangles represent samples L1, L2, and L3.

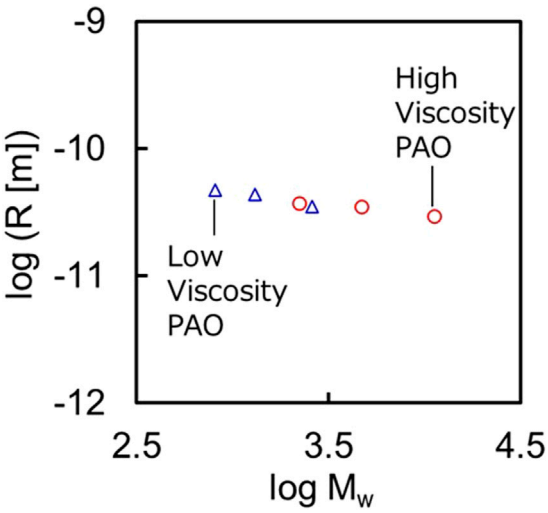

FIGURE 8
Relationship between R and M_w; Red circles represent samples H1, H2, and H3, while blue triangles represent samples L1, L2, and L3.

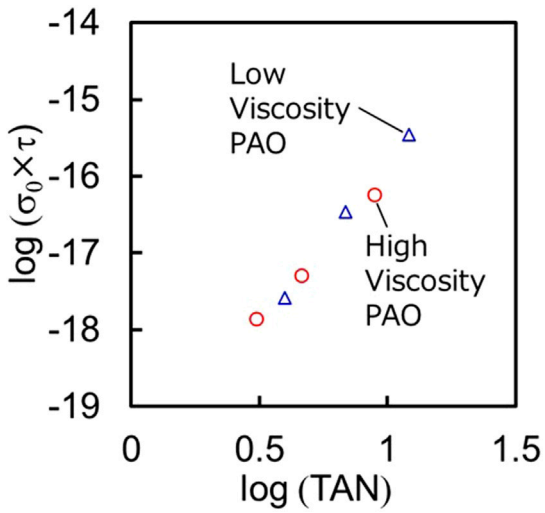

FIGURE 10
Relationship between $\sigma_0\tau$ and TAN; Red circles represent samples H1, H2, and H3, while blue triangles represent samples L1, L2, and L3.

Supplementary Table S1). As shown in Figure 7, τ generally increased proportionally to η, regardless of the initial viscosity of the sample. This result suggests that by calculating τ from DES measurements, it is possible to predict the viscosity of lubricating oil.

As shown in Figure 8, R remained nearly constant value regardless of the weight-average molecular weight, M_w of the degradation products. Although further validation of the accuracy of this value is necessary, it is evident that, at least in the dielectric relaxation phenomena caused by the oxidative degradation of PAO, the domains responding to the electric field are not the entire molecule but rather small units within the molecular chain. Furthermore, it is clear that this response is strongly correlated with the viscosity of the lubricant.

5.3 Relationship between β and PDI

The parameter β indicates the degree of distribution of relaxation times. When $\beta = 1$, this corresponds to a state where only a single relaxation mode is present. However, even in pure substances, β rarely equals 1 because dipoles interact with

surrounding molecules, and these interactions vary slightly depending on location. Moreover, in cases like the current study, where multiple relaxation species with different molecular weights and chemical structures exist within the system, β is expected to be smaller. The PDI represents the breadth of the molecular weight distribution of polymers, with larger values indicating greater dispersion. As the ester-based polymers generated by lubricant degradation follow a step-growth polymerization mechanism, it is expected that PDI will increase as degradation progresses.

Figure 9 shows the relationship between β and PDI. As degradation progressed, PDI increased and β decreased. This is likely due to the broadening of the molecular weight distribution and the increased complexity of the constituents as oxidative degradation progressed, resulting in an increase in the number of relaxation modes. On the other hand, when comparing the two types of oils, although the range of PDI variation differed significantly, there was no substantial difference in the range where the value of β existed. If the molecules themselves, generated by degradation, were aligning with the electric field, the plots for both oils in Figure 10 would overlap on the same line. Therefore, this result suggests that the size of the relaxation species is not significantly different between the two oils. As mentioned in section 5.2, this indicates that the dielectric relaxation is related to the movement of small segments within the polymer chains, and that these segments, as well as the surrounding environment, do not differ significantly between the two oils.

5.4 Relationship between σ_0, τ and TAN

TAN is a parameter that indicates the concentration of fatty acids produced by degradation and is widely used as an indicator of oxidative degradation of lubricants. Additionally, the concentration of fatty acids significantly affects the conductivity of the oil (Kajimoto et al., 2003), as it has been reported that the increase in ionicity is due to the high acid dissociation constant (Wada et al., 2014). The conductivity of a solution is generally expressed by equation Equation 11.

$$\sigma_0 = eN_c\mu_c \tag{11}$$

Here, e is the elementary charge, N_c represents the carrier concentration, and μ_c is the carrier mobility. Furthermore, using the Stokes-Einstein equation, it can be expressed in the form of Equation 12.

$$\sigma_0 = \frac{e^2N_c}{6\pi r\eta} \tag{12}$$

As mentioned in section 5.2, the viscosity of oxidatively degraded PAO is proportional to the relaxation time τ, leading to the derivation of the following equation.

$$\sigma_0\tau \propto \frac{N_c}{r} \tag{13}$$

Here, assuming that some of the carriers are fatty acid ions, N_c can be regarded as a function of TAN. Consequently, it is expected that $\sigma_0\tau$ would correlate with TAN. Therefore, when plotting the product of σ_0 and τ against TAN on a logarithmic scale, a single straight line was obtained, regardless of the initial viscosity (Figure 10).

This suggests that by utilizing two parameters observed in different frequency ranges, the degree of oxidative degradation of PAO can be diagnosed independently of the absolute value of viscosity. In other words, this method implies that when applied to lubricating oil films, it would be possible to diagnose oil degradation in a steady state where there is little change in oil film thickness. However, the plot in Figure 10 shows that $\sigma_0\tau$ depends on approximately the fourth power of TAN, suggesting that the carrier concentration in degraded oil is not solely determined by the concentration of fatty acid ions. There are likely other components that significantly contribute to the increase in conductivity. Potential causes may include the presence of ion species other than fatty acid ions in the degraded oil, as well as an increase in dissolved water content resulting from the increased polarity of the oil; however, the precise mechanisms remain unclear.

6 Conclusion

In this study, thermal degradation tests were conducted at 160°C using two types of poly (α-olefin) (PAO) with different viscosities to produce multiple samples with varying degrees of degradation. Dielectric spectroscopy (DES) with a parallel plate capacitor was applied to these samples to obtain detailed measurements of complex permittivity over a wide frequency range (30 Hz–1 MHz). The obtained dielectric relaxation parameters ($\varepsilon_{r\infty}$: permittivity at the high-frequency limit, $\Delta\varepsilon$: relaxation strength, τ: relaxation time, β: relaxation time distribution, and σ_0: DC conductivity) were thoroughly analyzed in relation to various properties derived from different analyses (η: viscosity, TAN: total acid number, C_d: mass concentration of degraded components, M_w: weight-average molecular weight, and PDI: polydispersity index). The following key findings were obtained:

1. It was demonstrated that $\Delta\varepsilon$ can be used to estimate the concentration of degradation products as a simple power function, regardless of the initial base oil viscosity. This is likely due to the fact that as the dipole concentration of degradation products increases, interactions among dipoles become significant, thereby affecting dielectric relaxation properties. This result suggests a new method for estimating the concentration of degradation products and evaluating the degree of lubricant degradation by measuring $\Delta\varepsilon$.
2. A proportional relationship between τ and η of the degraded oil was identified, consistent with Debye's theory, which states that relaxation time is proportional to the viscosity of the solution. Additionally, comparisons between τ and M_w, as well as between β and PDI, indicate that dielectric relaxation observed in oxidatively degraded PAO is due to the motion of small segments within polymer chains. These findings suggest that the viscosity of mixed oils with varying degradation levels can be estimated from τ.
3. The product of σ_0 and τ was found to correlate strongly with the TAN of degraded oil. This relationship is attributed to the fact that the conductivity of the oil is determined by the

concentration of ionic substances, such as fatty acids generated by oxidative degradation, as well as by the viscosity at that time. This result implies that by utilizing two parameters appearing at different frequency ranges, the degree of oxidative degradation of PAO can be diagnosed independently of absolute viscosity. In other words, this method can enable the diagnosis of oil degradation in a steady state with minimal changes in oil film thickness if applied to lubricating oil films.

These findings reveal that DES is an effective means of comprehensively evaluating lubricant degradation from the perspective of relaxation phenomena. Although further insights on pressure and temperature effects are needed to apply DES to oil film condition monitoring, the present results suggest the possibility of detecting early signs of lubrication failure, thus supporting the feasibility of implementing predictive maintenance (PdM) for bearings.

Data availability statement

The original contributions presented in the study are included in the article/supplementary material, further inquiries can be directed to the corresponding author.

Author contributions

SI: Writing–review and editing, Writing–original draft. TM: Writing–review and editing. SM: Writing–review and editing. SM: Writing–review and editing. FI: Writing–review and editing.

Funding

The author(s) declare that no financial support was received for the research, authorship, and/or publication of this article.

Acknowledgments

In writing this paper, I received valuable advice through discussions with Atsumi Koda of NSK Ltd. I would like to express my gratitude to her for the support.

Conflict of interest

Authors SI, TM, and SM were employed by NSK Ltd.

The remaining authors declare that the research was conducted in the absence of any commercial or financial relationships that could be construed as a potential conflict of interest.

Generative AI statement

The author(s) declare that no Generative AI was used in the creation of this manuscript.

Publisher's note

All claims expressed in this article are solely those of the authors and do not necessarily represent those of their affiliated organizations, or those of the publisher, the editors and the reviewers. Any product that may be evaluated in this article, or claim that may be made by its manufacturer, is not guaranteed or endorsed by the publisher.

Supplementary material

The Supplementary Material for this article can be found online at: https://www.frontiersin.org/articles/10.3389/fmech.2024.1504347/full#supplementary-material

References

Al-Badour, F., Sunar, M., and Cheded, L. (2011). Vibration analysis of rotating machinery using time–frequency analysis and wavelet techniques. *Mech. Syst. Signal Process.* 25 (6), 2083–2101. doi:10.1016/j.ymssp.2011.01.017

Becker-Dombrowsky, F. M., and Kirchner, E. (2024). Electrical impedance based condition monitoring of machine elements–a systematic review. *Frontiers* 10. doi:10.3389/fmech.2024.1412137

Böttcher, C. J. F., and Bordewijk, P. (1973). "Theory of electric polarization, vol. I," in *Dielectrics in static fields* (Amsterdam, Oxford, New York: Elsevier).

Böttcher, C. J. F., and Bordewijk, P. (1980). "Theory of electric polarization, vol. II," in *Dielectrics in time-dependent fields*. 2nd edn. (Amsterdam: Elsevier Science).

Cambow, R., Singh, M., Bagha, A. K., and Singh, H. (2018). To compare the effect of different level of self-lubrication for bearings using statistical analysis of vibration signal. *Mater. Today Proc.* 5 (14), 28364–28373. doi:10.1016/j.matpr.2018.10.121

Crook, A. W. (1961). Elastohydrodynamic lubrication of rollers. *Nature* 190, 1182–1183. doi:10.1038/1901182a0

Debye, P. (1929). *Polar molecules*. New York: Chemical Catalog Company.

Gong, Y., Guan, L., Feng, X., Zhou, J., Xu, X., and Wang, L. (2017). Low-temperature dielectric spectroscopy characterization of the oxidative degradation of lubricating oil. *Energy and Fuels* 31 (3), 2501–2512. doi:10.1021/acs.energyfuels.6b02795

Gong, Y., Guan, L., Wang, L., and Zhu, L. (2016). Two-channel and differential dielectric spectroscopy characterizationof lubricating oil. *Sensors Actuators A Phys.* 241, 74–86. doi:10.1016/j.sna.2016.02.013

Guan, L., Feng, X. L., Xiong, G., and Xie, J. A. (2011). Application of dielectric spectroscopy for engine lubricating oil degradation monitoring. *Sensors Actuators A Phys.* 168 (1), 22–29. doi:10.1016/j.sna.2011.03.033

Hamrock, B. J., and Dowson, D. (1977). Isothermal elastohydrodynamic lubrication of point contacts: Part III–Fully flooded results. *J. Lubr. Technol.* 99 (2), 264–275. doi:10.1115/1.3453074

Iwamoto, S., and Kumagai, H. (1998). Analysis of the dielectric relaxation of a gelatin solution. *Biosci. Biotechnol. Biochem.* 62 (7), 1381–1387. doi:10.1271/bbb.62.1381

Jablonka, K., Glovnea, R., and Bongaerts, J. (2012). Evaluation of EHD films by electrical capacitance. *J. Phys. D Appl. Phys.* 45 (38), 385301. doi:10.1088/0022-3727/45/38/385301

Johnston, G. J., Wayte, R., and Spikes, H. A. (1991). The measurement and study of very thin lubricant films in concentrated contacts. *Tribol. Trans.* 34 (2), 187–194. doi:10.1080/10402009108982026

Kajimoto, G., Nakamura, M., and Yamaguchi, M. (2003). Changes in organic acid components of volatile degradation products during oxidation of oil, and effects of organic acid on increased conductivity determined by the Rancimat method. *J. Jpn. Soc. Food Sci. Technol.* 50 (3), 223–229. doi:10.4327/jsnfs.50.223

Kaneta, M., Sakai, T., and Nishikawa, H. (1993). Effects of surface roughness on point contact EHL. *Tribol. Trans.* 36 (4), 605–612. doi:10.1080/10402009308983201

Kiral, Z., and Karagülle, H. (2003). Simulation and analysis of vibration signals generated by rolling element bearing with defects. *Tribol. Int.* 36 (9), 667–678. doi:10.1016/s0301-679x(03)00010-0

Kremer, F., and Schönhals, A. (2003). *Broadband dielectric spectroscopy* (Berlin: Springer).

Manabe, K., and Nakano, K. (2008). Breakdown of oil films and formation of residual films. *Tribol. Int.* 41 (11), 1103–1113. doi:10.1016/j.triboint.2008.02.001

Maruyama, T., Kosugi, D., Iwase, S., Maeda, M., Nakano, K., and Momozono, S. (2024). Application of the electrical impedance method to steel/steel EHD point contacts. *Frontiers* 10. doi:10.3389/fmech.2024.1489311

Maruyama, T., Maeda, M., and Nakano, K. (2019). Lubrication condition monitoring of practical ball bearings by electrical impedance method. *Tribol. Online* 14 (5), 327–338. doi:10.2474/trol.14.327

Maruyama, T., and Nakano, K. (2018). *In situ* quantification of oil film formation and breakdown in EHD contacts. *Tribol. Trans.* 61 (6), 1057–1066. doi:10.1080/10402004.2018.1468519

Maruyama, T., and Saitoh, T. (2010). Oil film behavior under minute vibrating conditions in EHL point contacts. *Tribol. Int.* 43, 1279–1286. doi:10.1016/j.triboint.2009.11.004

Nakano, K., and Akiyama, Y. (2006). Simultaneous measurement of film thickness and coverage of loaded boundary films with complex impedance analysis. *Tribol. Lett.* 22 (1), 127–134. doi:10.1007/s11249-006-9074-z

Nihira, T., Manabe, K., Tadokoro, C., Ozaki, S., and Nakano, K. (2015). Complex impedance measurement applied to short-time contact between colliding steel surfaces. *Tribol. Lett.* 57 (3), 29. doi:10.1007/s11249-015-0478-5

Patocka, F., Schneidhofer, C., Dörr, N., Schneider, M., and Schmid, U. (2020). 'Novel resonant MEMS sensor for the detection of particles withdielectric properties in aged lubricating oils. *Sensors Actuators A Phys.* 315, 112290. doi:10.1016/j.sna.2020.112290

Prashad, H. (1988). Theoretical evaluation of impedance, capacitance and charge accumulation on roller bearings operated under electrical fields. *Wear* 125 (3), 223–239. doi:10.1016/0043-1648(88)90115-9

Schnabel, S., Marklund, P., Minami, I., and Larsson, R. (2016). Monitoring of running-in of an EHL contact using contact impedance. *Tribol. Lett.* 63 (3), 35. doi:10.1007/s11249-016-0727-2

Sugimura, J., Jones, W. R., and Spikes, H. A. (1998). EHD film thickness in non-steady state contacts. *J. Tribol.* 120 (3), 442–452. doi:10.1115/1.2834569

Wada, J., Ueta, G., Okabe, S., and Amimoto, T. (2014). Method to evaluate the degradation condition of transformer insulating oil: experimental study on the hydrophilic and dissociative properties of degradation products. *IEEE Trans. Dielectr. Electr. Insulation* 21 (2), 873–881. doi:10.1109/tdei.2013.004204

Woodward, W. H. (2021). "Broadband dielectric spectroscopy—a practical guide," in *ACS symposium series* (Washington, DC: American Chemical Society).

Zarei, J., Tajeddini, M. A., and Karimi, H. R. (2014). Vibration analysis for bearing fault detection and classification using an intelligent filter. *Mechatronics* 24, 151–157. doi:10.1016/j.mechatronics.2014.01.003